Risk Prediction of RNA Off-Targets of CRISPR Base Editors in Tissue-Specific Transcriptomes Using Language Models

Kazuki Nakamae [1]*, Takayuki Suzuki [2], Sora Yonezawa [2], Kentaro Yamamoto [3], Taro Kakuzaki [4], Hiromasa Ono [1,5], Yuki Naito [5], and Hidemasa Bono [1,2,5]*

[1] Genome Editing Innovation Center, Hiroshima University, Higashi-Hiroshima, 739-0046, Japan; kazuki-nakamae@hiroshima-u.ac.jp; onohrms@hiroshima-u.ac.jp; bonohu@hiroshima-u.ac.jp
[2] Graduate School of Integrated Sciences for Life, Hiroshima University, Higashi-Hiroshima, 739-0046, Japan; d233528@hiroshima-u.ac.jp; d246887@hiroshima-u.ac.jp; bonohu@hiroshima-u.ac.jp
[3] Genome Analytics Japan Inc., Tokyo, 162-0067, Japan; yamaken37.the.answer@gmail.com
[4] Independent researcher; taro.kakuzaki@gmail.com
[5] Database Center for Life Science, Joint Support-Center for Data Science Research, Research Organization of Information and Systems, 178-4-4 Wakashiba, Kashiwa, 277-0871, Japan; hiromasa.ono@gmail.com; y-naito@dbcls.rois.ac.jp

* Correspondence: bonohu@hiroshima-u.ac.jp; Tel.: +81-82-424-4013 (H.B.); kazuki-nakamae@hiroshima-u.ac.jp; Tel.: +81-82-424-4013 (K.N.)

Abstract: Base-editing technologies, particularly cytosine base editors (CBEs), allow precise gene modification without introducing double-strand breaks; however, unintended RNA off-target effects remain a critical concern and are understudied. To address this gap, we developed PiCTURE, a standardized computational pipeline for detecting and quantifying transcriptome-wide CBE-induced RNA off-target events. PiCTURE identifies both canonical ACW (W = A or T/U) motif-dependent and non-canonical RNA off-targets, revealing a broader WCW motif that underlies many unanticipated edits. Additionally, we developed two machine learning models based on the DNABERT-2 language model, termed STL and SNL, which outperformed motif-only approaches in terms of accuracy, precision, recall, and F1 score. To demonstrate the practical application of our predictive model for CBE-induced RNA off-target risk, we integrated PiCTURE outputs with the PROTECTiO pipeline and estimated RNA off-target risk for each transcript showing tissue-specific expression. The analysis revealed differences among tissues: while the brain and ovaries exhibited relatively low off-target burden, the colon and lungs displayed relatively high risks. Our study provides a comprehensive framework for RNA off-target profiling, emphasizing the importance of advanced machine learning-based classifiers in CBE safety evaluations and offering valuable insights for the development of safer genome-editing therapies.

Keywords: CRISPR; base editing; RNA off-target; machine learning; tissue-specific transcriptome; PiCTURE; PROTECTiO

1. Introduction

Genome-editing technologies have revolutionized biological research and therapeutic strategies by enabling precise genetic modifications in various organisms [1–10]. CRISPR-based base editors (BEs) are particularly noteworthy for their ability to introduce site-specific nucleotide substitutions without causing double-strand breaks [8,9,11], which is particularly advantageous for introducing efficient substitutions in clinical *ex-vivo* and *in-vivo* applications [12–14]. Among BE tools, cytosine BEs (CBEs) have received attention for their capacity to convert cytosine (C) to uracil (U), which has the same base-pairing characteristics as thymine (T) in dsDNA [9,15], facilitating targeted gene knockout via the introduction of a premature stop codon and the correction of pathogenic single-nucleotide polymorphisms (SNPs)

[9,16]. However, several studies have reported that CBEs generate unintended C-to-U conversions in RNA, termed RNA off-target effects, which pose a potential safety concern [17–21]. Such RNA off-targets may elicit undesirable cellular responses, thereby compromising the safety and efficacy of CBE-based interventions.

While various strategies to mitigate RNA off-target effects have been developed [18–21], relatively little attention has been paid to the comprehensive, qualitative characterization of RNA off-target events. For example, canonical RNA off-targets often occur at known motifs, such as the ACW motif (where W represents A or T/U) [19,20]; however, non-canonical RNA off-targets that do not follow the ACW pattern remain poorly understood, and the field lacks a unified framework to systematically assess them. A thorough understanding of both canonical and non-canonical off-target events is critical for robust risk assessment and broader CBE applications.

To address this research gap, we developed the **Pi**peline for **C**RISPR-induced **T**ranscriptome-wide **U**nintended **R**NA **E**diting (**PiCTURE**), a standardized and quantitative platform designed to evaluate RNA off-target effects, including non-canonical events. To refine predictive capabilities for CBE-based RNA off-targets, we leveraged recent advances in machine learning, notably the emergence of language models such as DNABERT-2 [22]. By integrating the output of PiCTURE with a fine-tuned DNABERT-2 model, we established a robust framework for RNA off-target risk assessment. In addition, we introduce **P**redicting **R**NA **O**ff-target compared with **T**issue-specific **E**xpression for **C**aring for **Ti**ssue and **O**rgan (**PROTECTiO**), a framework that estimates tissue-wide off-target risks by analyzing transcriptomic data with tissue-specific expression profiles. Collectively, these approaches offer a standardized methodology for assessing RNA off-target risks, marking a significant step toward more reliable CBE-related safety evaluations and facilitating further advancements in base-editing specificity and therapeutic applicability.

2. Results and Discussion

2.1. A Uniform Pipeline for Detecting RNA Off-Targets

We first employed PiCTURE (Figure 1) to detect RNA off-target events in CBE-treated samples. We analyzed 13 RNA-sequencing (RNA-seq) datasets, including samples treated with nCas9, BE3, and BE4-rAPOBEC1, as reported previously [20,21]. Consistent with previous findings [20], our analysis of BE3-treated samples revealed numerous C-to-U(T) substitutions (corresponding to G-to-A on the complementary strand) (Supplementary Figure S1A,B). By evaluating the 101-bp sequences flanking these substituted cytosines, we identified sequence motifs that influence substrate specificity (Supplementary Figures S1A and S2A). Notably, the 5′ adjacent nucleotide strongly influenced the likelihood of C-to-U(T) conversions, with cytosines flanked by A or T (W) at the 5′ side being more frequently edited (Supplementary Figure S1A). Additionally, the 3′ adjacent nucleotide showed a weak bias toward A or T (W). Although a previous report highlighted the ACW motif to be associated with RNA off-targets [20], our findings suggest that a broader WCW motif may better capture the substrate preference for unintended RNA editing in human cells. The WCW motif has been recently reported in RNA off-targets in BE3 and YE1-BE3-FNLS transgenic mice [17], supporting our finding that CBE-based RNA off-targets preferentially lie within the WCW RNA motif.

To obtain further support for this observation, we performed the same analysis on samples treated with BE4-rAPOBEC1 or nCas9 (Supplementary Figure S2B). We considered samples treated with Cas9 as a negative control because the substitutions detected in the nCas9 samples were expected to result from spontaneous mutations in the transcriptome. Similar to BE3, BE4-rAPOBEC1-treated samples displayed motif-dependent C-to-U(T) substitutions, whereas no such motif enrichment was observed in the nCas9-treated samples. A comparison of the frequency of A or T nucleotides adjacent to converted Cs between BE4-rAPOBEC1 and nCas9 samples revealed a significantly higher frequency in the BE4-rAPOBEC1 samples than in the nCas9 samples (Supplementary Figure S2C). From these findings, it follows that, as noted above, not only the ACW motif but also related motifs such as TCW, WCA, and WCT—collectively represented by the broader WCW motif—can be interpreted as characteristic sequence contexts where BE3- and BE4-induced RNA off-target events occur frequently. A chromosome-wide analysis of C-to-U(T) conversions confirmed that BE4-rAPOBEC1-induced events were widely distributed (Supplementary Figure S3A,B) and significantly more abundant than those observed in nCas9-treated samples (Supplementary Figure S3C). These results demonstrate that PiCTURE enables the quantitative detection of C-to-U(T) substitutions, including CBE-induced RNA off-target events.

Next, we extracted datasets enriched for putative RNA off-targets from the identified C-to-U(T) conversion sites (Figure 2A). We first generated a negative dataset by collecting 40-bp or 101-bp sequences flanking each C-to-U(T) substitution site found in nCas9-treated replicates. We then generated a positive dataset from CBE-treated replicates by removing any sequences that overlapped with the negative dataset. For instance, using RNA-seq data from BE4-rAPOBEC1-transfected samples (SRR11561324, SRR11561298, and SRR11561273) and nCas9-transfected samples (SRR11561289, SRR11561314, and SRR11561326), we constructed a positive dataset. Among the 232,254 sequences in this positive dataset, 119,359 (51.4%) sequences contained the ACW motif (Figure 2B). Hereafter, we refer to these ACW-containing events as "canonical RNA off-targets," and those lacking the ACW motif as "non-canonical RNA off-targets." As mentioned above, we suggest that WCW motifs may also represent a key motif of unintended RNA editing. Indeed, examination of the positive dataset for the presence of WCW motifs showed that 159,545 out of 232,254 sequences (68.7%) contained a WCW motif (Figure 2B). This finding suggests that classification based on both ACW and WCW motifs may be valuable for detecting a broader range of CBE RNA off-targets.

2.2. Predicting RNA Off-Targets Using Nucleic Acid Language Models

We next aimed to construct a predictive model that does not solely rely on known motifs to identify RNA off-target-prone sequences. Recent advances in transformer-based nucleic acid language models [22–26] have enabled sophisticated sequence analyses. We adopted DNABERT-2 [22] as our base model and fine-tuned it using the negative and positive datasets derived from nCas9 and BE4-rAPOBEC1 samples, respectively, to develop a machine learning-based classifier for RNA off-target risk assessment (Figure 2C). First, we developed a model (hereafter referred to as the STL model) using datasets containing 78,944 positive and 21,790 negative sequences for training, 76,593 positive and 24,228 negative sequences for evaluation, and 76,717 positive and 23,476 negative sequences for testing. In each dataset, the positive samples outnumbered the negative samples by more than 3.1-fold, and some sequences were duplicated across datasets. Despite these imbalances and overlaps, the STL model achieved an accuracy above 0.8 and outperformed classifiers that rely solely on ACW, WCW, or nonspecific (NNN) motifs in terms of accuracy, precision, and F1-score (Table 1).

However, the WCW motif-based classifier achieved better recall. To improve the performance, we constructed a new dataset balanced for positive and negative sequences and without overlaps among the training, evaluation, and test sets. The new datasets contained 47,866 positive and 47,866 negative sequences for training, 10,257 positive and 10,257 negative sequences for evaluation, and 10,257 positive and 10,257 negative sequences for testing. We adjusted hyperparameters for better performance. We also shortened the input sequence length from 101 bp to 40 bp because we set "model_max_length" to 10 for our fine-tuning, and according to the DNABERT-2 manual, the recommended input sequence length should be four times "model_max_length." Under these conditions, we developed a second model, hereafter referred to as the SNL model, which outperformed the WCW motif-based classifier in all performance metrics (Table 2).

We then benchmarked the STL model, SNL model, and motif-based classifiers against canonical and non-canonical RNA off-targets. Using the SNL model's hold-out data (which were not used in training) to create datasets with and without the ACW motif, we randomly sampled 10 subsets and evaluated each classifier's performance (Figure 3). For Non-canonical RNA off-targets, the WCW motif-based classifier significantly outperformed the ACW motif-based classifier in all metrics, confirming the superiority of the WCW motif for detecting these events. Both the STL and SNL models significantly exceeded the performance of the WCW classifier in all metrics, demonstrating that language model-based predictions are particularly effective for detecting non-canonical RNA off-targets. The SNL model showed the highest accuracy, recall, and F1-score. Interestingly, the STL and SNL models also significantly outperformed motif-based classifiers for canonical RNA off-targets. While motif-based classifiers often exhibited very low precision (<0.3 on average), the STL and SNL models both achieved an average precision above 0.5, with the STL model reaching 0.72 on average. As precision reflects the proportion of predicted positives that are true positives, this improvement suggests that relying on motifs alone may lead to high false-positive rates. Although identifying motifs from RNA off-target data is valuable, using these motifs directly as predictors may inflate false positives. In contrast, the STL and SNL models produce fewer false positives and thus may prevent overestimating the RNA off-target risk associated with CBEs.

2.3. Assessment of Tissue-Specific CBE Risk Using Transcriptome Databases

In addition to motif-based classifiers, we successfully developed machine learning-based classifiers that operate independently of known motifs, enabling unconstrained RNA off-target risk prediction on any transcriptome sequence. To demonstrate this capability, we created a safety assessment pipeline, PROTECTiO (Figure 4), aimed at evaluating tissue- and organ-specific CBE RNA off-target risks. PROTECTiO employs a tissue-specific gene expression database, RefEx [27], derived from human RNA-seq data. For each gene with elevated expression in a specific tissue, we obtained its sequence and coding DNA sequence (CDS) information from the Ensembl database [28]. We then identified cytosine substrates (potential risk substrates; PRSs) whose conversion to U(T) could introduce a premature stop codon and truncate the encoded protein. Each PRS was evaluated using our CBE-induced RNA off-target classifiers. We defined substrates predicted as high-risk by our classifiers as effective PRSs. We then calculated the effective substrate density (ESD), i.e., the number of effective PRSs divided by the total number of PRSs and the transcript's amino acid length, and used the average ESD per tissue or organ as a representative measure of CBE-induced RNA off-target risk. When using the SNL model, we found that the brain, adipose tissue, ovaries, heart, and muscle exhibited significantly reduced RNA off-target risk compared with all transcripts showing tissue-specific expression, whereas the prostate, colon, and lungs showed significantly increased risk compared with all ones(Figure 5). Similar trends were observed with the ACW/WCW motif-based classifiers and the STL model, consistently indicating relatively low risk in the brain and ovaries and relatively high risk in the colon and lungs. The colon, in particular, showed notably high risk.

When we extracted colon-specific transcripts with ESD values exceeding the 95% confidence interval of a t-distribution constructed from all tissue-specific transcripts, we found a total of 505 transcripts across all four classifiers (Supplementary Figure S4). Of these, 202 transcripts (40%) were commonly identified by all four classifiers. The SNL model identified 365 colon-specific transcripts, including six unique transcripts not detected by the other classifiers. The ACW and WCW motif- and STL model-based classifiers identified 302 transcripts (24 unique), 380 transcripts (27 unique), and 393 transcripts (44 unique), respectively. We subjected these high-risk colon genes to Gene Ontology (GO) enrichment analyses to gain insight into their potential phenotypic impacts (Figure 6A, Supplementary Figure S5A–C). Seven GO terms, including GO:0095500, GO:1905145, GO:1905144, GO:0098926, GO:2000272, GO:0010469, and GO:0007267, were commonly enriched across all four classifiers (Figure 6B). These terms are associated with acetylcholine and signaling pathways. Specific high-risk genes, such as *LY6G6D* and *RGS10*, were related to some of these GO terms. Among the classifiers other than the ACW-based one, five common GO terms were enriched, including signaling-related terms such as GO:0038098, and a total of 14 GO terms were enriched in at least one non-ACW-based classifier. These results suggest that evaluating risk using only the ACW motif-based classifier, which suffers from both high false-positive and false-negative rates, may underestimate the true risk. Notably, we detected GO:0006978 (DNA damage response), whose status is obsolete, and the term was replaced by GO:0030330 on 2024-11-27, among the terms enriched in the SNL model. Recently, another group reported that in human hematopoietic stem/progenitor cells, the p53 response was lower for CBE (BE4max) than for Cas9 introduction [29]. A primary reason for this was likely the absence of double-strand breaks in CBE [30], whereas a minor possibility was that CBE-specific RNA off-target effects on transcripts associated with DNA damage response might affect the p53 response. Our results provide a foundation for designing more detailed follow-up analyses targeting *TP53* transcripts.

Notably, the STL and SNL models do not merely predict random substitution events but specifically target those derived from CBE-induced RNA off-target activity. The negative datasets used for the fine-tuning contained sequences that exhibited substitutions regardless of CBE introduction. In actual cellular environments, spontaneously occurring background mutations coexist with CBE-induced events, making it ideal—within a base-editing risk assessment context—to employ models designed to isolate the impact of CBE-driven substitutions, thereby neither overestimating nor underestimating the associated risk.

One technical consideration warrant further research. ll training data were derived from human RNA-seq datasets. While this approach is relevant for clinical applications of CBEs in humans, whether these findings can be generalized to other species remains to be validated. Despite the limitation, our study provides a quantifiable and standardized framework for assessing CBE-induced RNA off-target risks in human therapeutic contexts, forming a foundation for future research and broader CBE comparisons.

3. Materials and Methods

3.1. Implementation of PiCTURE

The PiCTURE pipeline comprises five steps: alignment, single-sample genotyping, joint genotyping, intersection, and mutation analysis (Figure 1).

PiCTURE processes RNA-seq data derived from base editing samples. After alignment, a BAM file is generated and converted into a VCF file, from which substitution mutations and motifs are extracted. PiCTURE can handle various input types. For example, when using VCF files obtained from joint genotyping, PiCTURE can receive multiple RNA-seq datasets as input. Users can also analyze intersected VCF files in the "Mutation analysis" section. The hg38 reference genome, index files, interval lists, and human dbSNP data are retrieved from the GATK [31] resource bundle (https://gatk.broadinstitute.org/hc/en-us/articles/360035890811-Resource-bundle).

PiCTURE can be run in both Docker [32] and Singularity (Apptainer) [33] containers, enabling operation on a variety of operating systems. Below, each process is described in detail.

3.1.1. Alignment

Quality control and adapter trimming are carried out using Trim Galore v0.6.7 with Cutadapt [34]. The trimmed RNA reads are aligned to the hg38 human genome with STAR aligner v2.7.4a [35], using a two-pass alignment. The output is a sorted BAM file. All reads in the sorted BAM file are assigned to a new read-group using AddOrReplaceReadGroups from Picard v2.3.0 [36]. Duplicate reads are marked with MarkDuplicatesSpark in GATK v4.3.0.0 [31]. Reads spanning splice junctions are split using SplitNCigarReads in GATK v4.3.0.0. Base quality recalibration is then carried out using baserecalibrator from GATK v4.3.0.0, generating a recalibration report, using the default setting for covariates and dbSNP build 138 [37] as a variant database for known sites.

3.1.2. Single-sample Genotyping

Genotypes are called using the HaplotypeCaller algorithm (-ERC GVCF) [38] in GATK v4.3.0.0 [31]. The variant calls from a single GVCF file are then aggregated into an efficient data structure via GenomicsDBImport in GATK v4.3.0.0. Subsequently, GenotypeGVCFs in GATK v4.3.0.0 is used for single-sample genotyping and to produce a single-sample VCF file.

3.1.3. Joint Genotyping

Genotypes are called using the HaplotypeCaller algorithm (-ERC GVCF) in GATK v4.3.0.0. The variant calls from multiple GVCF file are aggregated into an efficient data structure via GenomicsDBImport in GATK v4.3.0.0. GenotypeGVCFs in GATK v4.3.0.0 is used for joint genotyping, resulting in a multi-sample VCF file containing only high-confidence variants.

3.1.4. Intersection

An intersected VCF file can be obtained from the selected VCF files produced in sections 3.1.2 and 3.1.3. The selected VCF files are indexed with IndexFeatureFile in GATK v4.3.0.0. The indexed VCF files are compressed and merged using BCFtools v1.16 [39]. The intersected VCF is then extracted from the merged VCF file using SelectVariants (-select 'set == "Intersection";') in GATK v4.3.0.0].

3.1.5. Mutation Analysis

Substitutions are extracted from the output VCF file using SelectVariants (–-select-type-to-include SNP) from GATK v4.3.0.0. Next, substitutions are hard-filtered with VariantFiltration from GATK v4.3.0.0. A substitution is filtered out if it meets any of the following criteria: QualByDepth < 2, QUAL < 30, StrandOddsRatio > 3, FisherStrand > 60, RMS-MappingQuality < 40, MappingQualityRankSumTest < –12.5, ReadPosRandSumTest < –8.

Qualified substitutions are then classified by substitution class using PySam v0.19.1 [40]. Motifs are generated by analyzing the substitution site plus 50 bp upstream and downstream flanking sequences with WebLogo v3.7.12 [41]. Variant Allele Frequencies (VAFs) are calculated with BCFtools v1.16 [39] (fill-tags FORMAT/VAF) as the fraction of reads with the alternate allele. The VCF files are split according to VAF thresholds (e.g., VAF ≥0.8 or VAF <0.8), and motif generation is subsequently performed on these thresholded VCF files. The resulting substitution profiles are visualized using MultiQC v1.14 [42].

3.2. RNA-seq Dataset

The RNA-seq data were acquired from the Sequence Read Archive. We obtained SRR8096262 in PRJNA498065 as BE3 transfection data [20]. For the BE4-rAPOBEC1 transfection data, we collected SRR11561273, SRR11561298, SRR11561324, SRR11561299, SRR11561297, and SRR11561323 from PRJNA595157 [21]. Additionally, we procured SRR11561326, SRR11561314, SRR11561289, SRR11561325, SRR11561303, and SRR11561278 as nCas9 transfection data for the negative control. These RNA-seq data were obtained from cultured human HEK293T cells.

3.3. RNA Off-Target Analysis Using PiCTURE

All RNA-seq data were analyzed using the single-sample genotyping pipeline of PiCTURE. Nucleotide counts of substrates and their adjacent bases were aggregated from the statistical data output by the WebLogo function within PiCTURE. Statistical analyses with two-tailed Welch's t-test were conducted using custom Python scripts with SciPy [43]. Chromosome-scale visualization of variant allele frequency (VAF) data derived from substitution variants was achieved by processing the PiCTURE-generated VCF files with an R script using the “qqman” package [44]. All scripts were formatted for execution within a Snakemake workflow [45].

3.4. Preparation of the Fine-Tuning Dataset

For fine-tuning of the datasets, positive data were derived from RNA-seq samples transfected with BE3 or BE4-rAPOBEC1, whereas negative data were derived from RNA-seq samples transfected with nCas9. The construction of fine-tuning datasets for the STL and SNL models differed.

3.4.1. Fine-Tuning Dataset for the STL Model

For training data, we used positive data (88,040 sequences) from SRR11561298 and negative data (21,790 sequences) from SRR11561314. From these samples, PiCTURE first identified each C-to-T substitution site and then extracted a 101-bp flanking region—comprising 50 bp upstream and 50 bp downstream—for each substituted site. Among the positive sequences, those overlapping with negative sequences were removed from the positive set and retained as negative sequences. The 9,096 sequneces were removd from the positive set. As a result, the training dataset comprised 78,944 positive and 21,790 negative sequences.

For the evaluation dataset, we used positive data (86,908 sequences) from SRR11561273 and negative data (24,228 sequences) from SRR11561326. Sequences were extracted in the same manner as for the training data, and any sequences overlapping between the positive and negative sets were removed from the positive set and retained in the negative set. The 10,315 sequneces were removd from the positive set. This yielded 76,593 positive and 24,228 negative sequences for evaluation.

For the test dataset, we used positive data from SRR11561324 (86,417 sequences) and negative data (23,476 seqeunces) from SRR11561289. Applying the above procedure resulted in a test set of 76,717 positive and 23,476 negative sequences. The 9,700 sequneces were removd from the positive set due to overlaps.

3.4.2. Fine-Tuning Dataset for the SNL Model

First, we prepared a positive dataset by extracting C-to-T substitution sequences and their 20-bp upstream and 19-bp downstream flanking sequences from SRR8096262, SRR11561273, SRR11561297, SRR11561298, SRR11561299, SRR11561323, and SRR11561324, using PiCTURE. The sequences were merged into a single FASTA file (691,376 sequences). Similarly, we extracted negative data sequences from SRR11561278, SRR11561289, SRR11561303, SRR11561314, SRR11561325, and SRR11561326, and merged them into another FASTA file (139,187). We then removed duplicate sequences within positive_40bp.fa and negative_40bp.fa, using SeqKit v2.3.0 (rmdup) [46]. 155,474 and 70,807 sequences were removed from the positive_40bp.fa and negative_40bp.fa, respectively.

Next, we used a custom Python script to identify sequences duplicated between the positive and negative sets. 26,461 duplicate sequences were removed from the positive data and retained in the negative data. Using the train_test_split function in scikit-learn v1.3.0 [47], we split the positive and negative data at a ratio of 7:1.5:1.5 to create training, evaluation, and test datasets, respectively. We further balanced the datasets so that each subset contained equal numbers of positive and negative sequences. The final training, evaluation, and test datasets contained 47,866 positive and 47,866 negative sequences, 10,257 positive and 10,257 negative sequences, and 10,257 positive and 10,257 negative sequences, respectively.

3.5. Fine-Tuning a Pre-Trained Language Model for Predicting CBE-Based RNA Off-Targets

We fine-tuned the DNABERT-2 model (zhihan1996/DNABERT-2-117M from the Hugging Face repository) [22] to create a classifier capable of detecting C-to-U substitutions induced by CBEs on RNA, yielding two models: the STL model and the SNL model.

3.5.1. Fine-Tuning Parameters for the STL Model

The total number of original sequences from PiCURE output was 330,859 sequences. The sequence dataset was split by RNA-seq data and filtered as described in Section 3.4.1. We used 78,944, 76,593, and 76,717 sequences for training, evaluation, and test as positive datasets, respectively. We also used 21,790, 24,228, and 23,476 sequences for training, evaluation, and test as negative datasets, respectively.

We fine-tuned zhihan1996/DNABERT-2-117M, with the following parameters: model_max_length = 10, per_device_train_batch_size = 10, per_device_eval_batch_size = 16, gradient_accumulation_steps = 1, learning_rate = 3e-5, fp16 = TRUE, num_train_epochs = 10, save_steps = 200, evaluation_strategy = steps, eval_steps = 200, warmup_steps = 55, and logging_steps = 100.

3.5.2. Fine-Tuning Parameters for the SNL Model

The total number of original sequences from PiCURE output was 830,563 sequences. The sequence dataset was split by positive and negative labels and filtered as described in Section 3.4.2. We used 47,866, 10,257, and 10,257 sequences for training, evaluation, and test as positive datasets, respectively. We also used 47,866, 10,257, and 10,257 sequences for training, evaluation, and test as negative datasets, respectively.

We fine-tuned zhihan1996/DNABERT-2-117M, with the following parameters: model_max_length = 10, per_device_train_batch_size = 8, per_device_eval_batch_size = 16, gradient_accumulation_steps = 8, learning_rate = 2e-5, fp16 = TRUE, num_train_epochs = 8, save_steps = 200, evaluation_strategy = steps, eval_steps = 200, warmup_steps = 50, and logging_steps = 100.

Accuracy, precision, recall, and F1 scores for the fine-tuned models were obtained from the output of the DNABERT-2 train.py script. Additionally, we evaluated accuracy, precision, recall, and F1 scores for ACW, WCW, and NNN motif-based models using the test data via a custom script that leveraged scikit-learn v1.4.2.

The STL model (https://huggingface.co/KazukiNakamae/STLmodel) and SNL model (https://huggingface.co/KazukiNakamae/SNLmodel) were deposited on the Hugging Face platform [48].

3.6. Comparing Classifier Performance for Canonical and Non-canonical RNA Off-Targets

Using custom Python scripts, we collected 20,514 sequences (40 bp each) from the SNL model test dataset and divided them into positive and negative sets. Within each set, the sequences were further divided into those with and those without the ACW motif, generating a canonical RNA off-target dataset with 4,987 positive and 1,498 negative sequences, and a non-canonical RNA off-target dataset with 5,270 positive and 8,759 negative sequences. Both datasets were evaluated using the ACW and WCW motif classifiers and the STL and SNL models.

After performing the predictions, we randomly selected 1,000 positive and 1,000 negative sequences from each dataset, fixing the random seed for reproducibility. Using scikit-learn v1.5.1, we calculated the accuracy, precision, recall, and F1 scores. We then aggregated these results and conducted two-tailed Welch's t-test using SciPy v1.10.1.

3.7. Tissue-Specific Risk Assessment Using PROTECTiO

We applied PROTECTiO to evaluate how CBE-induced RNA off-target events might affect genes with tissue- or organ-specific elevated expression.

First, we obtained tissue-specific expression patterns that were pre-calculated from Illumina bodyMap2 transcriptome RNAseq data (PRJEB2445) in RefEx (https://refex.dbcls.jp) [27]], a curated gene expression reference dataset. This dataset is publicly available at https://dx.doi.org/10.6084/m9.figshare.4028709. The expression patterns were organized by NCBI RefSeq IDs [49], with tissue specificity indicated by binary values (1: tissue-specific high expression, -1: tissue-specific low expression). We then retrieved the corresponding Ensembl transcript IDs for each NCBI RefSeq [49] ID using the TogoID [50] API. Using the Ensembl [28] REST API, we obtained CDS coordinate and genomic sequence information for each transcript and reconstructed the CDS sequences. From these CDS sequences, we deduced amino acid sequences and identified PRSs, i.e., cytosine residues whose C-to-U substitution could introduce a premature stop codon.

For each PRS identified, we retrieved the 20-bp upstream and 19-bp downstream flanking sequences from the genomic coordinates and listed them using Ensembl [28] transcript ID. We then evaluated these sequences with the ACW and WCW motif classifiers and STL and SNL model classifiers, classifying any PRS predicted as positive by a classifier as an effective PRS. To compute the ESD, we summed the numbers of effective PRSs per transcript and normalized the sums to the total number of PRSs in that transcript and to the length (in amino acids) of the encoded protein.

We aggregated ESD values per tissue and conducted two-tailed t-test using SciPy v1.10.1 and statsmodels v0.14.1 [51]. Transcripts whose ESD exceeded the 95% confidence interval of a t-distribution constructed from all tissue-specific transcripts were defined as high-risk genes. The transcript list was exported as a CSV file.

3.8. Enrichment Analysis of High-Risk Genes

We input the list of high-risk genes generated by PROTECTiO into ShinyGO 0.81 (http://bioinformatics.sdstate.edu/go/) [52] for enrichment analysis. We focused only on GO [53] terms related to Biological Processes, setting the FDR cutoff at 0.05 and pathway size between 2 and 2,000. For ontology analysis, we used the “simona” v1.2.0

package [54], computing term similarity using the "Sim_WP_1994" method [55]. Word clouds were generated using the "simplifyEnrichment" package [56], and an UpSet plot was created using the "Complexupset " package [57].

4. Conclusions

We developed PiCTURE, a standardized pipeline for analyzing CBE-induced RNA off-targets, and successfully detected both canonical (ACW motif-containing) and non-canonical RNA off-targets. By integrating language model-based machine learning, we accurately predicted non-canonical RNA off-target events, overcoming limitations of motif-only classifiers. When applying our models to different human tissues, the results suggested a relatively low RNA off-target risk in the brain and ovaries and a relatively high risk in the colon and lungs. This tissue-specific risk information can serve as a valuable resource for predicting potential side effects of CBEs and guiding safety evaluations in clinical applications.

Supplementary Materials: Supplementary Figure S1: Overview of substitution patterns and motif preferences identified by PiCTURE; Supplementary Figure S2: Motif preferences associated with C-to-U conversions in BE3 and BE4-rAPOBEC1 samples compared to nCas9 negative controls; Supplementary Figure S3: Chromosomal distribution and abundance of C-to-U conversions in BE4-rAPOBEC1 and nCas9 samples; Supplementary Figure S4: Overlap of high-risk genes identified by motif-based and machine learning-based classifiers; Supplementary Figure S5. Gene Ontology (GO) enrichment analyses for high-risk gene subsets identified by different classifiers.

Author Contributions: Conceptualization, K.N., H.O., and Y.N.; methodology, K.N., T.S., T.K., and S.Y.; software, K.N. and T.S.; validation, K.N.; formal analysis, K.N. and S.Y.; investigation, K.N. and Y.N.; resources, K.N. S.T., and H.O.; data curation, K.N.; writing—original draft preparation, K.N.; writing—review and editing, H.B.; visualization, K.N., S.Y., and K.Y.; supervision, H.B.; project administration, K.N.; funding acquisition, K.N. and H.B. All authors have read and agreed to the published version of the manuscript.

Funding: This research was funded by ROIS-DS-JOINT 2022 [grant number 030RP2022 to K.N.], ROIS-DS-JOINT 2023 [grant number 009RP2023 to K.N.], and ROIS-DS-JOINT 2024 [grant number 012RP2024 to H.B.]. This work was also supported by the Center of Innovation for Bio-Digital Transformation (BioDX), an open innovation platform for industry–academia cocreation (COI-NEXT) and the Japan Science and Technology Agency (JST) [grant number JPMJPF2010 to K.N. and H.B.).

Institutional Review Board Statement: Not applicable

Informed Consent Statement: Not applicable

Data Availability Statement: Publicly available datasets were analyzed in this study. The script for PiCTURE and the associated scripts are available here: https://github.com/KazukiNakamae/PiCTURE (accessed on 21 December 2024). The STL model is available here: https://huggingface.co/KazukiNakamae/STLmodel (accessed on 21 December 2024). The SNL model is available here: https://huggingface.co/KazukiNakamae/SNLmodel (accessed on 21 December 2024). The script for PROTECTiO and the associated scripts are available here: https://github.com/KazukiNakamae/PROTECTiO (accessed on 21 December 2024). The transcript-level evaluation data generated by PROTECTiO are publicly available here: https://doi.org/10.6084/m9.figshare.28053845.v1 (accessed on 21 December 2024).

Acknowledgments: Computations were partially performed on the NIG supercomputer at ROIS National Institute of Genetics. We would like to thank all laboratory members at Hiroshima University for their valuable comments.

Conflicts of Interest: K.N. and H.O. were employed by PtBio Inc.

Abbreviations

The following abbreviations are used in this manuscript:

CBE, cytosine base editor

PiCTURE, Pipeline for CRISPR-induced Transcriptome-wide Unintended RNA Editing

PROTECTiO, Predicting RNA Off-target compared with Tissue-specific Expression for Caring for Tissue and Organ

RNA-seq, RNA-sequencing

SNP, single-nucleotide polymorphism

References

1. Zong, Y.; Liu, Y.; Xue, C.; Li, B.; Li, X.; Wang, Y.; Li, J.; Liu, G.; Huang, X.; Cao, X.; et al. An Engineered Prime Editor with Enhanced Editing Efficiency in Plants. *Nat Biotechnol* **2022**, *40*, 1394–1402, doi:10.1038/s41587-022-01254-w.
2. McAuley, G.E.; Yiu, G.; Chang, P.C.; Newby, G.A.; Campo-Fernandez, B.; Fitz-Gibbon, S.T.; Wu, X.; Kang, S.-H.L.; Garibay, A.; Butler, J.; et al. Human T Cell Generation Is Restored in CD3δ Severe Combined Immunodeficiency through Adenine Base Editing. *Cell* **2023**, *186*, 1398-1416.e23, doi:10.1016/j.cell.2023.02.027.
3. Urnov, F.D.; Miller, J.C.; Lee, Y.-L.; Beausejour, C.M.; Rock, J.M.; Augustus, S.; Jamieson, A.C.; Porteus, M.H.; Gregory, P.D.; Holmes, M.C. Highly Efficient Endogenous Human Gene Correction Using Designed Zinc-Finger Nucleases. *Nature* **2005**, *435*, 646–651, doi:10.1038/nature03556.
4. Li, T.; Huang, S.; Zhao, X.; Wright, D.A.; Carpenter, S.; Spalding, M.H.; Weeks, D.P.; Yang, B. Modularly Assembled Designer TAL Effector Nucleases for Targeted Gene Knockout and Gene Replacement in Eukaryotes. *Nucleic Acids Research* **2011**, *39*, 6315–6325, doi:10.1093/nar/gkr188.
5. Platt, R.J.; Chen, S.; Zhou, Y.; Yim, M.J.; Swiech, L.; Kempton, H.R.; Dahlman, J.E.; Parnas, O.; Eisenhaure, T.M.; Jovanovic, M.; et al. CRISPR-Cas9 Knockin Mice for Genome Editing and Cancer Modeling. *Cell* **2014**, *159*, 440–455, doi:10.1016/j.cell.2014.09.014.
6. Nakade, S.; Tsubota, T.; Sakane, Y.; Kume, S.; Sakamoto, N.; Obara, M.; Daimon, T.; Sezutsu, H.; Yamamoto, T.; Sakuma, T.; et al. Microhomology-Mediated End-Joining-Dependent Integration of Donor DNA in Cells and Animals Using TALENs and CRISPR/Cas9. *Nat Commun* **2014**, *5*, 5560, doi:10.1038/ncomms6560.
7. Suzuki, K.; Tsunekawa, Y.; Hernandez-Benitez, R.; Wu, J.; Zhu, J.; Kim, E.J.; Hatanaka, F.; Yamamoto, M.; Araoka, T.; Li, Z.; et al. In Vivo Genome Editing via CRISPR/Cas9 Mediated Homology-Independent Targeted Integration. *Nature* **2016**, *540*, 144–149, doi:10.1038/nature20565.
8. Nishida, K.; Arazoe, T.; Yachie, N.; Banno, S.; Kakimoto, M.; Tabata, M.; Mochizuki, M.; Miyabe, A.; Araki, M.; Hara, K.Y.; et al. Targeted Nucleotide Editing Using Hybrid Prokaryotic and Vertebrate Adaptive Immune Systems. *Science* **2016**, *353*, aaf8729, doi:10.1126/science.aaf8729.
9. Komor, A.C.; Kim, Y.B.; Packer, M.S.; Zuris, J.A.; Liu, D.R. Programmable Editing of a Target Base in Genomic DNA without Double-Stranded DNA Cleavage. *Nature* **2016**, *533*, 420–424, doi:10.1038/nature17946.
10. Anzalone, A.V.; Randolph, P.B.; Davis, J.R.; Sousa, A.A.; Koblan, L.W.; Levy, J.M.; Chen, P.J.; Wilson, C.; Newby, G.A.; Raguram, A.; et al. Search-and-Replace Genome Editing without Double-Strand Breaks or Donor DNA. *Nature* **2019**, *576*, 149–157, doi:10.1038/s41586-019-1711-4.
11. Gaudelli, N.M.; Komor, A.C.; Rees, H.A.; Packer, M.S.; Badran, A.H.; Bryson, D.I.; Liu, D.R. Programmable Base Editing of A•T to G•C in Genomic DNA without DNA Cleavage. *Nature* **2017**, *551*, 464–471, doi:10.1038/nature24644.
12. Gaudelli, N.M.; Lam, D.K.; Rees, H.A.; Solá-Esteves, N.M.; Barrera, L.A.; Born, D.A.; Edwards, A.; Gehrke, J.M.; Lee, S.-J.; Liquori, A.J.; et al. Directed Evolution of Adenine Base Editors with Increased Activity and Therapeutic Application. *Nat Biotechnol* **2020**, *38*, 892–900, doi:10.1038/s41587-020-0491-6.
13. Georgiadis, C.; Rasaiyaah, J.; Gkazi, S.A.; Preece, R.; Etuk, A.; Christi, A.; Qasim, W. Base-Edited CAR T Cells for Combinational Therapy against T Cell Malignancies. *Leukemia* **2021**, *35*, 3466–3481, doi:10.1038/s41375-021-01282-6.
14. Musunuru, K.; Chadwick, A.C.; Mizoguchi, T.; Garcia, S.P.; DeNizio, J.E.; Reiss, C.W.; Wang, K.; Iyer, S.; Dutta, C.; Clendaniel, V.; et al. In Vivo CRISPR Base Editing of PCSK9 Durably Lowers Cholesterol in Primates. *Nature* **2021**, *593*, 429–434, doi:10.1038/s41586-021-03534-y.
15. Komor, A.C.; Zhao, K.T.; Packer, M.S.; Gaudelli, N.M.; Waterbury, A.L.; Koblan, L.W.; Kim, Y.B.; Badran, A.H.; Liu, D.R. Improved Base Excision Repair Inhibition and Bacteriophage Mu Gam Protein Yields C:G-to-T:A Base Editors with Higher Efficiency and Product Purity. *Science Advances* **2017**, *3*, eaao4774, doi:10.1126/sciadv.aao4774.

16. Billon, P.; Bryant, E.E.; Joseph, S.A.; Nambiar, T.S.; Hayward, S.B.; Rothstein, R.; Ciccia, A. CRISPR-Mediated Base Editing Enables Efficient Disruption of Eukaryotic Genes through Induction of STOP Codons. *Mol Cell* **2017**, *67*, 1068-1079.e4, doi:10.1016/j.molcel.2017.08.008.
17. Yan, N.; Feng, H.; Sun, Y.; Xin, Y.; Zhang, H.; Lu, H.; Zheng, J.; He, C.; Zuo, Z.; Yuan, T.; et al. Cytosine Base Editors Induce Off-Target Mutations and Adverse Phenotypic Effects in Transgenic Mice. *Nat Commun* **2023**, *14*, 1784, doi:10.1038/s41467-023-37508-7.
18. Grünewald, J.; Zhou, R.; Iyer, S.; Lareau, C.A.; Garcia, S.P.; Aryee, M.J.; Joung, J.K. CRISPR DNA Base Editors with Reduced RNA Off-Target and Self-Editing Activities. *Nat Biotechnol* **2019**, *37*, 1041–1048, doi:10.1038/s41587-019-0236-6.
19. Zhou, C.; Sun, Y.; Yan, R.; Liu, Y.; Zuo, E.; Gu, C.; Han, L.; Wei, Y.; Hu, X.; Zeng, R.; et al. Off-Target RNA Mutation Induced by DNA Base Editing and Its Elimination by Mutagenesis. *Nature* **2019**, *571*, 275–278, doi:10.1038/s41586-019-1314-0.
20. Grünewald, J.; Zhou, R.; Garcia, S.P.; Iyer, S.; Lareau, C.A.; Aryee, M.J.; Joung, J.K. Transcriptome-Wide off-Target RNA Editing Induced by CRISPR-Guided DNA Base Editors. *Nature* **2019**, *569*, 433–437, doi:10.1038/s41586-019-1161-z.
21. Yu, Y.; Leete, T.C.; Born, D.A.; Young, L.; Barrera, L.A.; Lee, S.-J.; Rees, H.A.; Ciaramella, G.; Gaudelli, N.M. Cytosine Base Editors with Minimized Unguided DNA and RNA Off-Target Events and High on-Target Activity. *Nat Commun* **2020**, *11*, 2052, doi:10.1038/s41467-020-15887-5.
22. Zhou, Z.; Ji, Y.; Li, W.; Dutta, P.; Davuluri, R.; Liu, H. DNABERT-2: Efficient Foundation Model and Benchmark For Multi-Species Genome 2024.
23. Sanabria, M.; Hirsch, J.; Joubert, P.M.; Poetsch, A.R. DNA Language Model GROVER Learns Sequence Context in the Human Genome. *Nat Mach Intell* **2024**, *6*, 911–923, doi:10.1038/s42256-024-00872-0.
24. Yang, M.; Huang, L.; Huang, H.; Tang, H.; Zhang, N.; Yang, H.; Wu, J.; Mu, F. Integrating Convolution and Self-Attention Improves Language Model of Human Genome for Interpreting Non-Coding Regions at Base-Resolution. *Nucleic Acids Res* **2022**, *50*, e81, doi:10.1093/nar/gkac326.
25. Ji, Y.; Zhou, Z.; Liu, H.; Davuluri, R.V. DNABERT: Pre-Trained Bidirectional Encoder Representations from Transformers Model for DNA-Language in Genome. *Bioinformatics* **2021**, *37*, 2112–2120, doi:10.1093/bioinformatics/btab083.
26. Dalla-Torre, H.; Gonzalez, L.; Mendoza-Revilla, J.; Lopez Carranza, N.; Grzywaczewski, A.H.; Oteri, F.; Dallago, C.; Trop, E.; de Almeida, B.P.; Sirelkhatim, H.; et al. Nucleotide Transformer: Building and Evaluating Robust Foundation Models for Human Genomics. *Nat Methods* **2024**, 1–11, doi:10.1038/s41592-024-02523-z.
27. Ono, H.; Ogasawara, O.; Okubo, K.; Bono, H. RefEx, a Reference Gene Expression Dataset as a Web Tool for the Functional Analysis of Genes. *Sci Data* **2017**, *4*, 170105, doi:10.1038/sdata.2017.105.
28. Harrison, P.W.; Amode, M.R.; Austine-Orimoloye, O.; Azov, A.G.; Barba, M.; Barnes, I.; Becker, A.; Bennett, R.; Berry, A.; Bhai, J.; et al. Ensembl 2024. *Nucleic Acids Res* **2023**, *52*, D891–D899, doi:10.1093/nar/gkad1049.
29. Fiumara, M.; Ferrari, S.; Omer-Javed, A.; Beretta, S.; Albano, L.; Canarutto, D.; Varesi, A.; Gaddoni, C.; Brombin, C.; Cugnata, F.; et al. Genotoxic Effects of Base and Prime Editing in Human Hematopoietic Stem Cells. *Nat Biotechnol* **2024**, *42*, 877–891, doi:10.1038/s41587-023-01915-4.
30. Ferrari, S.; Jacob, A.; Beretta, S.; Unali, G.; Albano, L.; Vavassori, V.; Cittaro, D.; Lazarevic, D.; Brombin, C.; Cugnata, F.; et al. Efficient Gene Editing of Human Long-Term Hematopoietic Stem Cells Validated by Clonal Tracking. *Nat Biotechnol* **2020**, *38*, 1298–1308, doi:10.1038/s41587-020-0551-y.
31. McKenna, A.; Hanna, M.; Banks, E.; Sivachenko, A.; Cibulskis, K.; Kernytsky, A.; Garimella, K.; Altshuler, D.; Gabriel, S.; Daly, M.; et al. The Genome Analysis Toolkit: A MapReduce Framework for Analyzing next-Generation DNA Sequencing Data. *Genome Res* **2010**, *20*, 1297–1303, doi:10.1101/gr.107524.110.
32. Merkel, D. Docker: Lightweight Linux Containers for Consistent Development and Deployment. *Linux J.* **2014**, *2014*, 2:2.
33. Kurtzer, G.M.; Sochat, V.; Bauer, M.W. Singularity: Scientific Containers for Mobility of Compute. *PLOS ONE* **2017**, *12*, e0177459, doi:10.1371/journal.pone.0177459.

34. Martin, M. Cutadapt Removes Adapter Sequences from High-Throughput Sequencing Reads. *EMBnet.journal* **2011**, *17*, 10–12, doi:10.14806/ej.17.1.200.
35. Dobin, A.; Davis, C.A.; Schlesinger, F.; Drenkow, J.; Zaleski, C.; Jha, S.; Batut, P.; Chaisson, M.; Gingeras, T.R. STAR: Ultrafast Universal RNA-Seq Aligner. *Bioinformatics* **2013**, *29*, 15–21, doi:10.1093/bioinformatics/bts635.
36. Picard Tools - By Broad Institute Available online: http://broadinstitute.github.io/picard/ (accessed on 27 December 2024).
37. Sherry, S.T.; Ward, M.-H.; Kholodov, M.; Baker, J.; Phan, L.; Smigielski, E.M.; Sirotkin, K. dbSNP: The NCBI Database of Genetic Variation. *Nucleic Acids Res* **2001**, *29*, 308–311.
38. Poplin, R.; Ruano-Rubio, V.; DePristo, M.A.; Fennell, T.J.; Carneiro, M.O.; Auwera, G.A.V. der; Kling, D.E.; Gauthier, L.D.; Levy-Moonshine, A.; Roazen, D.; et al. Scaling Accurate Genetic Variant Discovery to Tens of Thousands of Samples 2018, 201178.
39. Li, H. A Statistical Framework for SNP Calling, Mutation Discovery, Association Mapping and Population Genetical Parameter Estimation from Sequencing Data. *Bioinformatics* **2011**, *27*, 2987–2993, doi:10.1093/bioinformatics/btr509.
40. Pysam-Developers/Pysam 2024.
41. Crooks, G.E.; Hon, G.; Chandonia, J.-M.; Brenner, S.E. WebLogo: A Sequence Logo Generator. *Genome Res* **2004**, *14*, 1188–1190, doi:10.1101/gr.849004.
42. Ewels, P.; Magnusson, M.; Lundin, S.; Käller, M. MultiQC: Summarize Analysis Results for Multiple Tools and Samples in a Single Report. *Bioinformatics* **2016**, *32*, 3047–3048, doi:10.1093/bioinformatics/btw354.
43. Virtanen, P.; Gommers, R.; Oliphant, T.E.; Haberland, M.; Reddy, T.; Cournapeau, D.; Burovski, E.; Peterson, P.; Weckesser, W.; Bright, J.; et al. SciPy 1.0: Fundamental Algorithms for Scientific Computing in Python. *Nat Methods* **2020**, *17*, 261–272, doi:10.1038/s41592-019-0686-2.
44. Turner, S.D. Qqman: An R Package for Visualizing GWAS Results Using Q-Q and Manhattan Plots. *Journal of Open Source Software* **2018**, *3*, 731, doi:10.21105/joss.00731.
45. Mölder, F.; Jablonski, K.P.; Letcher, B.; Hall, M.B.; Tomkins-Tinch, C.H.; Sochat, V.; Forster, J.; Lee, S.; Twardziok, S.O.; Kanitz, A.; et al. Sustainable Data Analysis with Snakemake 2021.
46. Shen, W.; Sipos, B.; Zhao, L. SeqKit2: A Swiss Army Knife for Sequence and Alignment Processing. *iMeta* **2024**, *3*, e191, doi:10.1002/imt2.191.
47. Pedregosa, F.; Varoquaux, G.; Gramfort, A.; Michel, V.; Thirion, B.; Grisel, O.; Blondel, M.; Prettenhofer, P.; Weiss, R.; Dubourg, V.; et al. Scikit-Learn: Machine Learning in Python. *Journal of Machine Learning Research* **2011**, *12*, 2825–2830.
48. Wolf, T.; Debut, L.; Sanh, V.; Chaumond, J.; Delangue, C.; Moi, A.; Cistac, P.; Rault, T.; Louf, R.; Funtowicz, M.; et al. HuggingFace's Transformers: State-of-the-Art Natural Language Processing 2020.
49. O'Leary, N.A.; Wright, M.W.; Brister, J.R.; Ciufo, S.; Haddad, D.; McVeigh, R.; Rajput, B.; Robbertse, B.; Smith-White, B.; Ako-Adjei, D.; et al. Reference Sequence (RefSeq) Database at NCBI: Current Status, Taxonomic Expansion, and Functional Annotation. *Nucleic Acids Res* **2016**, *44*, D733–D745, doi:10.1093/nar/gkv1189.
50. Ikeda, S.; Ono, H.; Ohta, T.; Chiba, H.; Naito, Y.; Moriya, Y.; Kawashima, S.; Yamamoto, Y.; Okamoto, S.; Goto, S.; et al. TogoID: An Exploratory ID Converter to Bridge Biological Datasets. *Bioinformatics* **2022**, *38*, 4194–4199, doi:10.1093/bioinformatics/btac491.
51. Seabold, S.; Perktold, J. Statsmodels: Econometric and Statistical Modeling with Python. *scipy* **2010**, doi:10.25080/Majora-92bf1922-011.
52. Ge, S.X.; Jung, D.; Yao, R. ShinyGO: A Graphical Gene-Set Enrichment Tool for Animals and Plants. *Bioinformatics* **2020**, *36*, 2628–2629, doi:10.1093/bioinformatics/btz931.
53. Aleksander, S.A.; Balhoff, J.; Carbon, S.; Cherry, J.M.; Drabkin, H.J.; Ebert, D.; Feuermann, M.; Gaudet, P.; Harris, N.L.; Hill, D.P.; et al. The Gene Ontology Knowledgebase in 2023. *Genetics* **2023**, *224*, iyad031, doi:10.1093/genetics/iyad031.
54. Gu, Z. Simona: A Comprehensive R Package for Semantic Similarity Analysis on Bio-Ontologies. *BMC Genomics* **2024**, *25*, 869, doi:10.1186/s12864-024-10759-4.

55. Wu, Z.; Palmer, M. Verb Semantics and Lexical Selection 1994.
56. Gu, Z.; Hübschmann, D. simplifyEnrichment: A Bioconductor Package for Clustering and Visualizing Functional Enrichment Results. *Genomics Proteomics Bioinformatics* **2023**, *21*, 190–202, doi:10.1016/j.gpb.2022.04.008.
57. Conway, J.R.; Lex, A.; Gehlenborg, N. UpSetR: An R Package for the Visualization of Intersecting Sets and Their Properties. *Bioinformatics* **2017**, *33*, 2938–2940, doi:10.1093/bioinformatics/btx364.

Table and figure legends

Table 1. Performance comparison of motif-based classifiers and the STL model for RNA off-target prediction.

Table 2. Performance comparison of motif-based classifiers and the SNL model for RNA off-target prediction.

Figure 1. Overview of the PiCTURE pipeline for RNA off-target analysis. The PiCTURE workflow for detecting and characterizing CBE-induced RNA off-target events is shown. (1) Input RNA-seq data from base editing samples undergo quality control, adapter trimming, and two-pass alignment to the hg38 reference genome. After alignment, duplicate fragments are marked, reads spanning splice junctions are split, and base quality scores are recalibrated using the dbSNP database, resulting in an analysis-ready BAM file. (2A) In single-sample genotyping, variants are called from the analysis-ready BAM file, producing a GVCF file and, after genotyping, a single-sample VCF file. (2B) For joint genotyping, variants from multiple GVCFs are combined to generate a multi-sample VCF, and (2C) intersected VCF files can be produced by selecting variants common to multiple conditions. (3) During mutation analysis, SNVs are filtered, and motif analyses are conducted using the integrated tools in PiCTURE, yielding final outputs such as substitution profiles and sequence motif representations.

Figure 2. Conceptual workflow for CBE-based RNA off-target motif identification and the fine-tuning of a language model. The process for identifying and characterizing RNA off-target events caused by CBEs and subsequently integrating this information into a machine learning framework is shown. (A) Starting from RNA-seq data, PiCTURE detects numerous C-to-U conversions, which can be classified into canonical and non-canonical RNA off-targets based on the ACW motif. (B) The numbers of RNA off-targets associated with ACW and WCW motifs are quantified and compared. (C) The sequence datasets from PiCTURE are then used to fine-tune the DNABERT-2 model for predicting CBE-induced RNA off-targets. The DNABERT-2 model used is pre-trained on a large-scale genomic corpus (32.49B nucleotide bases from a multi-species genome dataset) created by another group (Zhou *et al*., 2024[22]).

Figure 3. Performance comparison of motif- and language model-based classifiers for canonical and non-canonical RNA off-target detection. Box plots show the accuracy, precision, recall, and F1 score distributions for the ACW and WCW motif classifiers and STL and SNL models. Each classifier's performance was evaluated using datasets containing canonical (ACW motif) and noncanonical (no ACW motif) RNA off-targets. Asterisks indicate $p < 0.05$ with two-tailed Welch's t-test and "n.s." denotes no significant difference.

Figure 4. Overview of the PROTECTiO pipeline for tissue-specific RNA off-target risk assessment. The workflow employed by PROTECTiO to evaluate tissue-specific CBE-induced RNA off-target risks is shown. Tissue-specific gene expression data were retrieved from RefEx and mapped to corresponding Ensembl transcript IDs via TogoID in the ID conversion process. Using the Ensembl REST API, CDSs and associated genomic coordinates were obtained, enabling the extraction of CDS sequences. Each candidate cytosine (C), named PRS, that could form a premature stop codon when deaminated was identified using the CDS and genomic sequences, and PRS flanking sequences were evaluated using various classifiers (motif- or language model-based) for CBE-induced RNA off-target prediction. The results were then processed to calculate the ESD for the transcript. The formula used to calculate the ESD, which reflects the relative abundance of effective PRSs in each transcript, is provided in the right box. Finally, all effective substrates corresponding to transcripts significantly upregulated in at least one tissue or organ were grouped by tissue type, and two-tailed Welch's t-test was then performed to estimate organ- and tissue-specific RNA off-target risks.

Figure 5. Tissue-specific ESD illustrating RNA off-target risk. The bar plot displays the average ESD of transcripts with standard error of the mean across various human tissues. The "All" column lists transcripts that are tissue-specifically upregulated or down-regulated in at least one of the tissues and organs. The other columns list tissue-specific active transcripts, which are upregulated transcripts in the tissues or organs. Lower ESD values indicate reduced predicted RNA off-target risk, whereas higher values suggest an elevated risk. "n" represents the number of transcripts. Asterisks indicate $p < 0.05$ with two-tailed Welch's t-test. The illustrations are from TogoTV (© 2016 DBCLS TogoTV, CC-BY-4.0).

Figure 6. Enrichment analysis of GO terms associated with high-risk genes identified by multiple classifiers. Summary of enrichment analysis. (A) The figure presents Gene Ontology (GO) enrichment analyses for high-risk, colon-specific transcripts (genes) identified by the SNL model. The plot shows enriched GO Biological Process terms along with their fold enrichment and significance (-log10(FDR)). Each bar corresponds to a GO term, color-coded according to its –log10(FDR) value, while the dot size indicates the number of associated genes. The N represents the number of high-risk colon-specific transcripts. (B) The upset plot of GO terms commonly enriched in different classifier sets. Colored bars represent the count of GO terms found in one or more classifier sets (SNL model, STL model, WCW motif, and ACW motif). Dots with connecting lines indicate classifier combinations.

Tables

Table 1

	Accuracy	Precision	Recall	F1 Score
STL model	0.803	0.729	0.672	0.690
ACW motif classifier	0.596	0.636	0.686	0.580
WCW motif classifier	0.703	0.663	0.721	0.662
NNN motif classifier	0.766	0.383	0.5	0.434

Table 2

	Accuracy	Precision	Recall	F1 Score
SNL model	0.726	0.729	0.726	0.725
ACW motif classifier	0.670	0.697	0.670	0.659
WCW motif classifier	0.717	0.717	0.717	0.716
NNN motif classifier	0.5	0.25	0.5	0.333

Figures

Figure 1

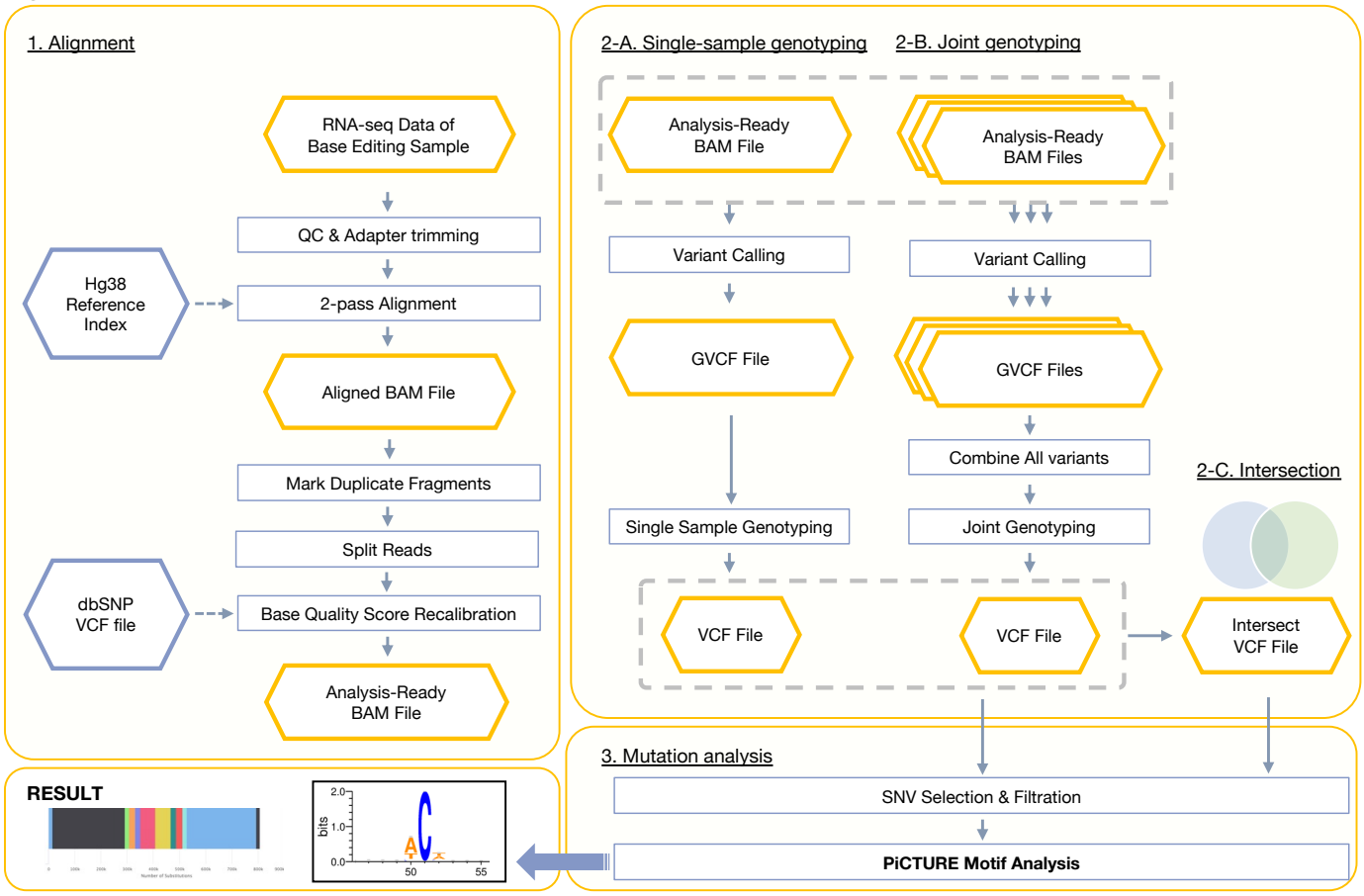

Figure 2

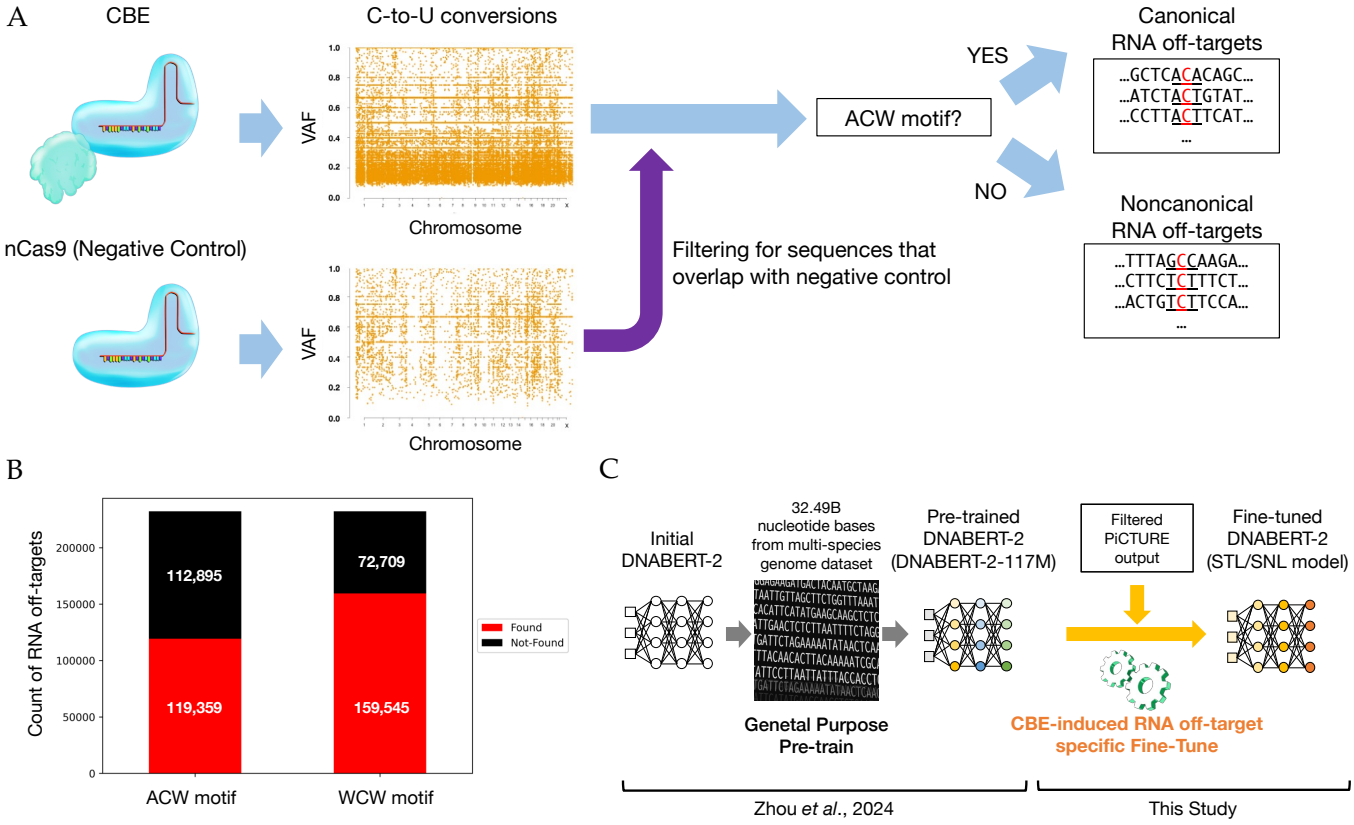
A
CBE
C-to-U conversions
VAF
Chromosome
nCas9 (Negative Control)
VAF
Chromosome
ACW motif?
YES
NO
Canonical
RNA off-targets
...GCTCACACAGC...
...ATCTACTGTAT...
...CCTTACTTCAT...
...
Noncanonical
RNA off-targets
...TTTAGCCAAGA...
...CTTCTCTTTCT...
...ACTGTCTTCCA...
...
Filtering for sequences that
overlap with negative control
B
Count of RNA off-targets
200000
150000
100000
50000
0
112,895
119,359
72,709
159,545
Found
Not-Found
ACW motif
WCW motif
C
Initial
DNABERT-2
32.49B
nucleotide bases
from multi-species
genome dataset
Pre-trained
DNABERT-2
(DNABERT-2-117M)
Filtered
PiCTURE
output
Fine-tuned
DNABERT-2
(STL/SNL model)
Genetal Purpose
Pre-train
CBE-induced RNA off-target
specific Fine-Tune
Zhou et al., 2024
This Study

Figure 3

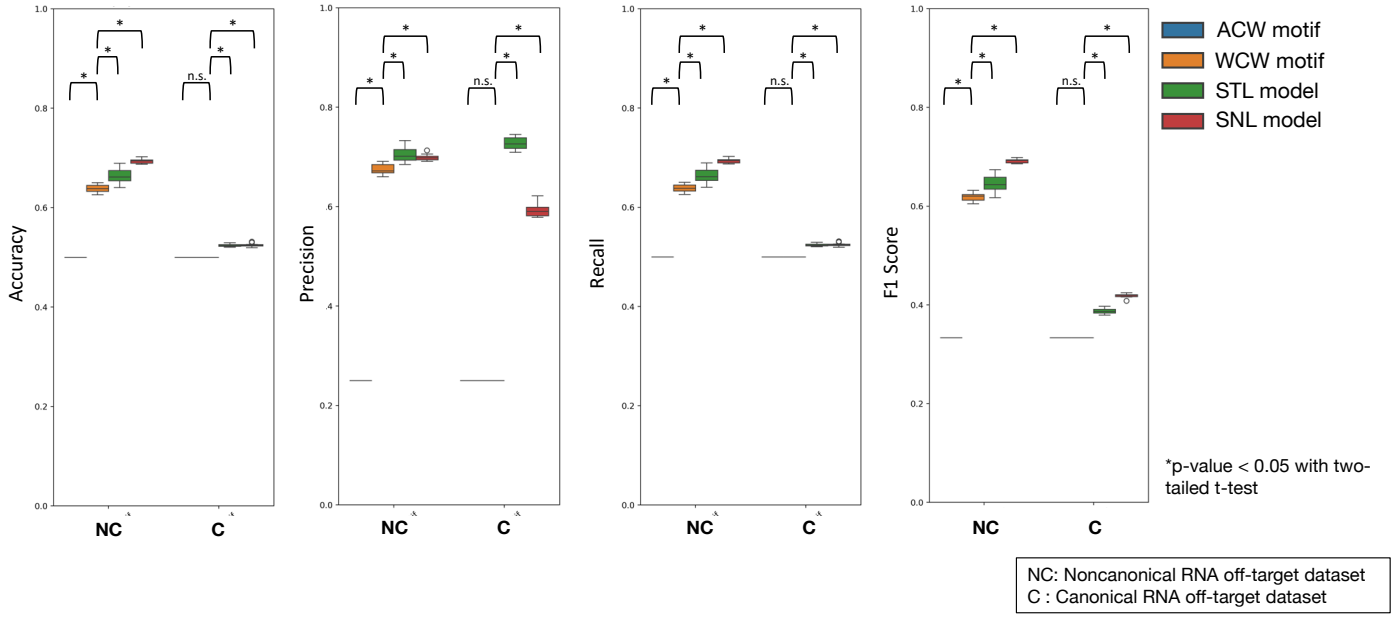
Accuracy
Precision
Recall
F1 Score
NC
C
n.s.
ACW motif
WCW motif
STL model
SNL model
*p-value < 0.05 with two-tailed t-test
NC: Noncanonical RNA off-target dataset
C : Canonical RNA off-target dataset

Figure 4

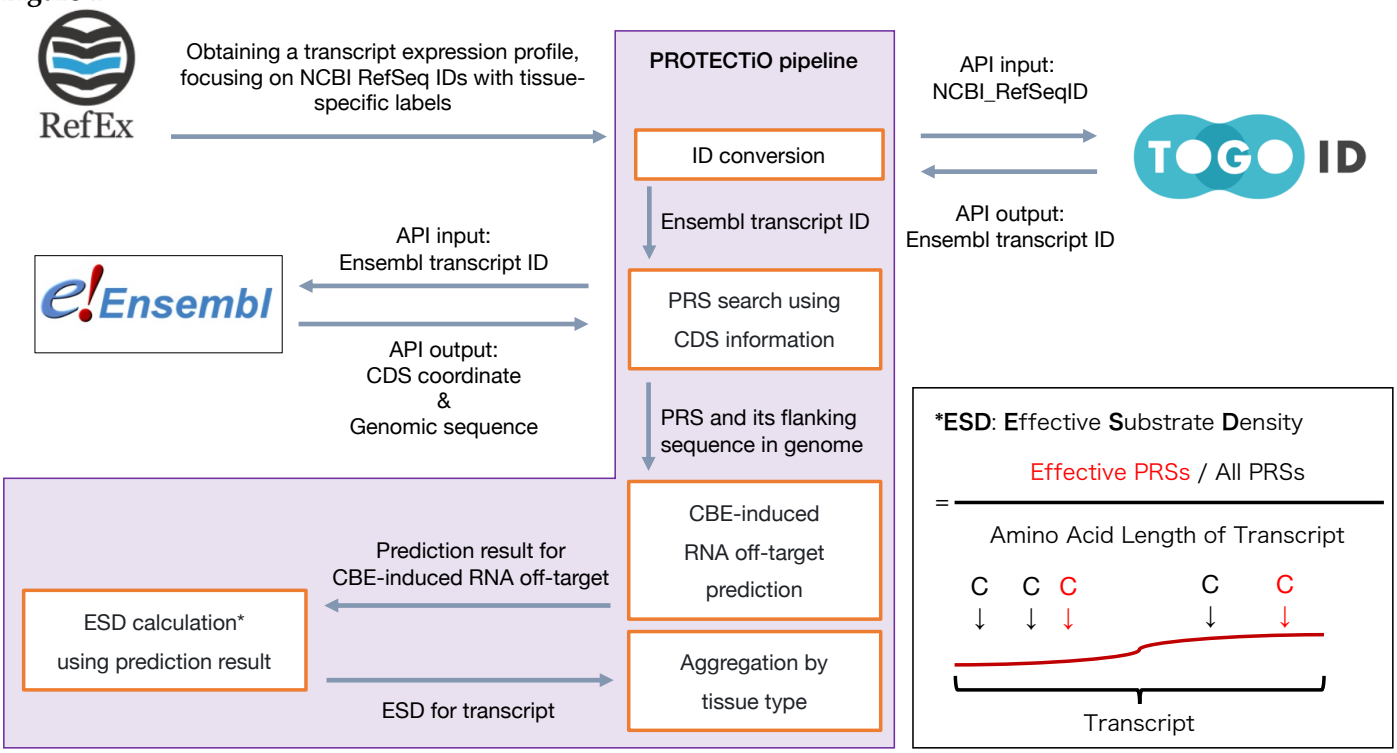
RefEx
Obtaining a transcript expression profile, focusing on NCBI RefSeq IDs with tissue-specific labels
PROTECTiO pipeline
ID conversion
Ensembl transcript ID
PRS search using CDS information
PRS and its flanking sequence in genome
CBE-induced RNA off-target prediction
Aggregation by tissue type
API input: NCBI_RefSeqID
API output: Ensembl transcript ID
TOGO ID
Ensembl
API input: Ensembl transcript ID
API output: CDS coordinate & Genomic sequence
Prediction result for CBE-induced RNA off-target
ESD calculation* using prediction result
ESD for transcript
*ESD: Effective Substrate Density
Effective PRSs / All PRSs
Amino Acid Length of Transcript
C C C C C
Transcript

Figure 5

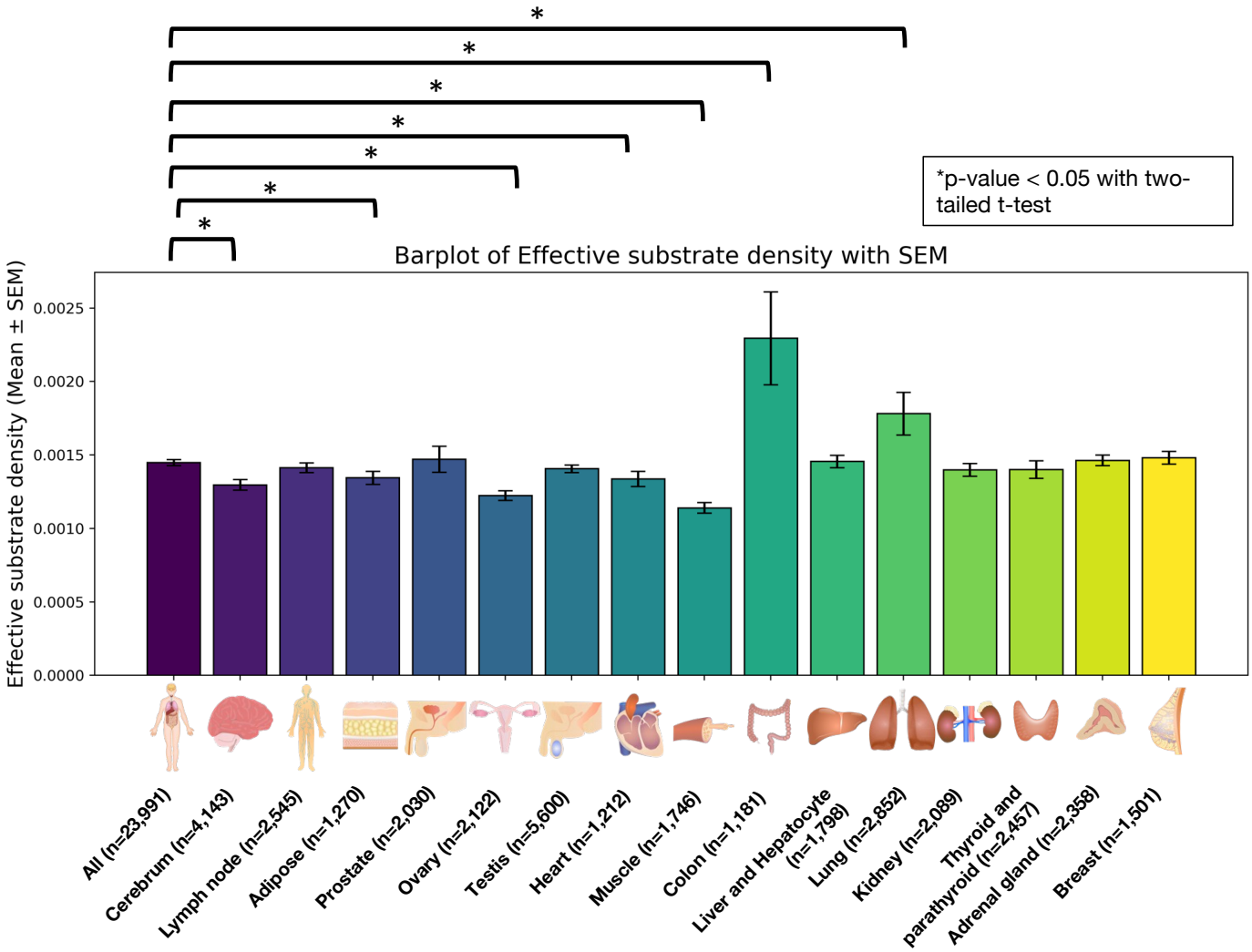
*
*
*
*
*
*
*
*p-value < 0.05 with two-tailed t-test
Barplot of Effective substrate density with SEM
Effective substrate density (Mean ± SEM)
0.0025
0.0020
0.0015
0.0010
0.0005
0.0000
All (n=23,991)
Cerebrum (n=4,143)
Lymph node (n=2,545)
Adipose (n=1,270)
Prostate (n=2,030)
Ovary (n=2,122)
Testis (n=5,600)
Heart (n=1,212)
Muscle (n=1,746)
Colon (n=1,181)
Liver and Hepatocyte (n=1,798)
Lung (n=2,852)
Kidney (n=2,089)
Thyroid and parathyroid (n=2,457)
Adrenal gland (n=2,358)
Breast (n=1,501)

Figure 6

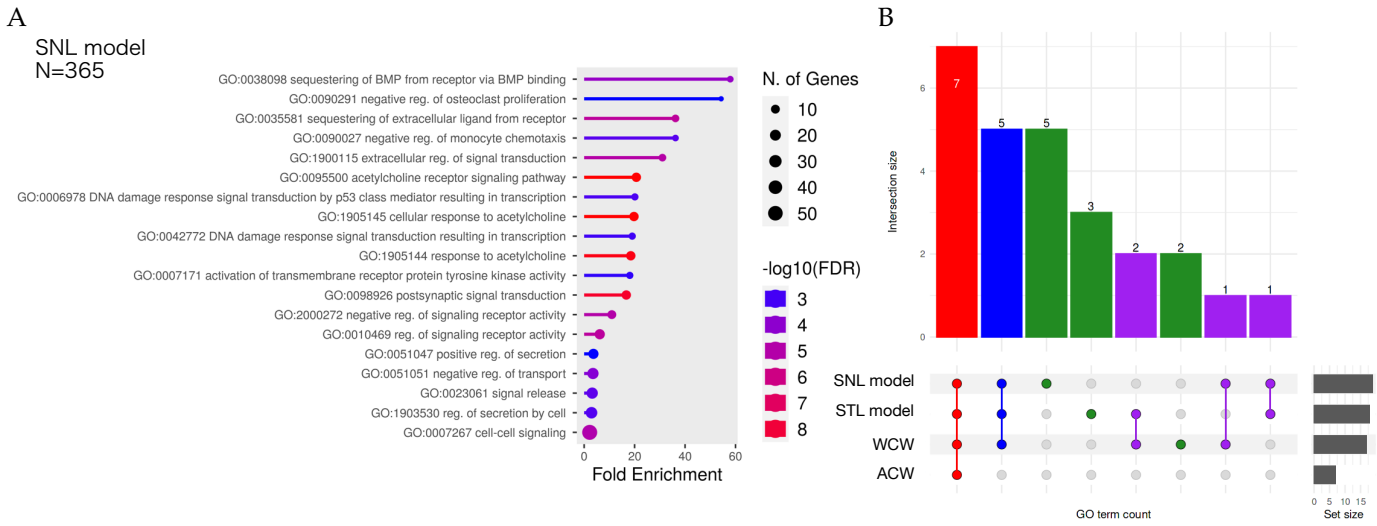
A
SNL model
N=365
GO:0038098 sequestering of BMP from receptor via BMP binding
GO:0090291 negative reg. of osteoclast proliferation
GO:0035581 sequestering of extracellular ligand from receptor
GO:0090027 negative reg. of monocyte chemotaxis
GO:1900115 extracellular reg. of signal transduction
GO:0095500 acetylcholine receptor signaling pathway
GO:0006978 DNA damage response signal transduction by p53 class mediator resulting in transcription
GO:1905145 cellular response to acetylcholine
GO:0042772 DNA damage response signal transduction resulting in transcription
GO:1905144 response to acetylcholine
GO:0007171 activation of transmembrane receptor protein tyrosine kinase activity
GO:0098926 postsynaptic signal transduction
GO:2000272 negative reg. of signaling receptor activity
GO:0010469 reg. of signaling receptor activity
GO:0051047 positive reg. of secretion
GO:0051051 negative reg. of transport
GO:0023061 signal release
GO:1903530 reg. of secretion by cell
GO:0007267 cell-cell signaling
0
20
40
60
Fold Enrichment
N. of Genes
10
20
30
40
50
-log10(FDR)
3
4
5
6
7
8
B
Intersection size
7
5
5
3
2
2
1
1
SNL model
STL model
WCW
ACW
GO term count
Set size